



PROCEEDINGS OF SPIE  
SPIE—The International Society for Optical Engineering

# ***Laser Techniques for Surface Science III***

**Hai-Lung Dai  
Hans-Joachim Freund**  
*Chairs/Editors*

**29–31 January 1998  
San Jose, California**

*Sponsored and Published by*  
SPIE—The International Society for Optical Engineering



**Volume 3272**

SPIE is an international technical society dedicated to advancing engineering and scientific applications of optical, photonic, imaging, electronic, and optoelectronic technologies.

# Laser-Induced Desorption of NO from NiO(100): *Ab initio*- and Wave Packet Calculations

T. Klüner<sup>a</sup>, S. Thiel<sup>a</sup>, H.-J. Freund<sup>a</sup>, and V. Staemmler<sup>b</sup>

<sup>a</sup>Fritz-Haber-Institut der Max-Planck-Gesellschaft,  
Faradayweg 4-6, 14195 Berlin, Germany

<sup>b</sup>Ruhr-Universität Bochum, Lehrstuhl für Theoretische Chemie,  
Universitätsstr. 150, 44780 Bochum, Germany

## ABSTRACT

In this paper we discuss theoretical investigations of UV-laserinduced desorption of NO-molecules from Nickeloxide-(100)-surfaces. We focus on the interpretation of experimental results (velocity-distributions of the desorbing molecules, rotational and vibrational distributions) by performing for the first time high quality *ab initio* configuration interaction (CI) calculations for the construction of two dimensional potential energy surfaces of the ground and excited states involved in the desorption process.

We were able to characterise these states as charge transfer states, where an electron is transferred from the surface into the NO- $2\pi$ -orbital. Potential energy surfaces for the intermediate NO<sup>-</sup>-like states have been constructed by varying the molecule-surface distance and the tilt angle of the molecule axis with respect to the surface normal. The characterisation of the potential energy surfaces allows for a mechanistic insight into the driving forces of nuclear motion.

Three dimensional wave packet calculations on the *ab initio* potential surfaces have been performed to simulate the experimentally obtained state resolved velocity distributions of the desorbing NO-molecules. It has been possible to simulate experimental details like desorption cross sections, bimodal velocity distributions and the coupling of rotational and translational degrees of freedom on the basis of our first principles calculations.

**Keywords:** theory of DIET, wavepacket dynamics, *ab initio* calculations

## 1. INTRODUCTION

State resolved laser induced desorption of small molecules from well-characterized metal or oxide surfaces has become a very active field of fundamental research during the recent years<sup>1</sup>. Many experimental studies yield a great amount of detailed results, which are mostly interpreted by classical or semi-classical models<sup>2</sup>. Quantum-mechanical descriptions have also been presented<sup>3-7</sup> but, in general, a quantitative simulation of experimental results suffers from the lack of sufficiently accurate potential energy surfaces (PES) especially for the excited electronic states involved in the desorption process.

Recently, the very first calculation of excited states involved in the 'desorption induced by electronic transitions' (DIET) process for the system NO/NiO(100) has been reported<sup>8</sup>. A characterisation of these states has been performed<sup>9</sup> and an analytical expression of a representative PES has been presented<sup>10</sup>. In the present paper, the selection of a representative excited state of the cluster/adsorbate system and its efficient calculation on the basis of a configuration interaction (CI) approach is discussed.

The *ab initio* calculated PES are used as the basis of three-dimensional (3D) wave packet calculations which allow for a direct comparison with experimental results such as rotationally-vibrationally state resolved velocity distributions of the desorbing NO-molecules. The experimental investigations have been performed by Mull et al.<sup>11</sup> and the main results are presented in figure 1, where velocity distribution of the desorbing NO-molecules in different rotational/vibrational states are illustrated.

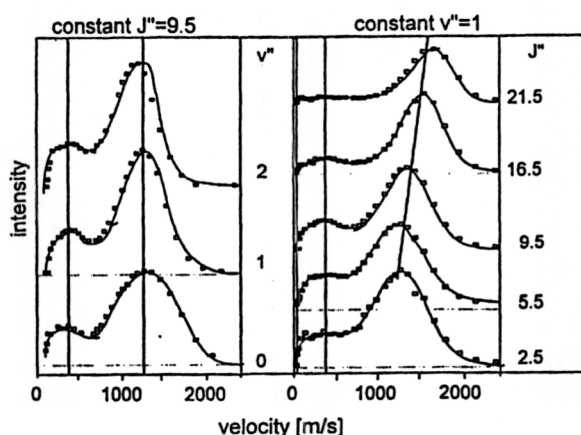


Figure 1. Experimental velocity distributions of NO molecules after laser induced desorption from NiO(100) for different rotational and vibrational quantum numbers<sup>11</sup>.

As a characteristic feature of all velocity distributions a bimodality is observed consisting of two non-thermal desorption channels. Additionally, a decoupling of the internal NO-vibration and the translation of desorbing NO-molecules is indicated by the similarity of all velocity distributions for different vibrational quanta but for a constant rotational quantum number ( $J''=9.5$ , left side of figure 1). Obviously, the NO-vibration is not a relevant coordinate in order to understand the shape of the velocity distributions, so that in quantum chemical calculations this coordinate can be neglected in a first approximation. Therefore, in the construction of potential energy surfaces the NO-distance is fixed to be  $r_{\text{NO}}=2.175 \text{ a}_0$  according to the NO gas phase value<sup>8</sup>. In contrast to this, a coupling of rotation and translation in the fast desorption channel is observed for a constant vibrational quantum number ( $v''=1$ , right side of figure 1). Therefore, the rotation of the NO-molecule has to be included in all simulations of the experimental velocity distributions.

## 2. METHODS OF CALCULATION

### 2.1 QUANTUM CHEMICAL CALCULATIONS

The NiO(100) surface is represented by a cluster model containing a  $\text{NiO}_5^{8-}$ -cluster embedded in a semi-infinite Madelung potential of point charges ( $\pm 2$ ). In the fcc lattice structure the distance between the cations and anions is chosen to reproduce the experimental value of about  $3.93 \text{ a}_0$ <sup>12</sup>. The cluster model including an adsorbed NO-molecule is shown in figure 2.

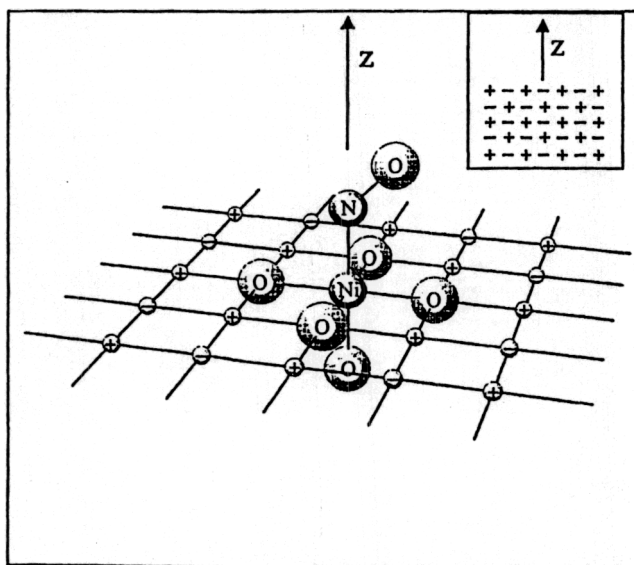


Figure 2. The  $\text{NiO}_5^{8-}$ -cluster embedded in a semi-infinite potential of point charges (only the uppermost layer is shown).

All *ab initio* calculations have been performed with the Bochum open-shell program package using restricted open shell Hartree Fock (ROHF)<sup>13</sup>, complete active space self-consistent field (CASSCF)<sup>14</sup> and configuration interaction (CI)<sup>15</sup> programs. The basis set used consists of a 13s6p4d basis of Roos et al.<sup>16</sup>, a 7s3p basis of Huzinaga<sup>17</sup>, contracted to double zeta quality for the O<sup>2-</sup>-ions and a 9s5p basis of Huzinaga<sup>17</sup> for nitrogen and oxygen of the NO molecule, contracted to triple zeta quality. The basis set for the NO-molecule has been extended by one diffuse p-set with the exponents 0.05 and 0.06, respectively. Furthermore, the basis of the O<sup>2-</sup> cluster ions is extended by a semidiffuse s- and p-set with an exponent of 0.1 in order to describe the larger spatial extend of the wavefunction compared to neutral oxygen atoms.

In order to construct an appropriate reference determinant for the subsequent configuration interaction calculations of the intermediate excited states the experimental evidence of NO<sup>-</sup> being the intermediate during laser induced desorption has to be considered<sup>11</sup>. The NO<sup>-</sup>-like character of the excited states is controversially discussed<sup>9,18</sup> but detailed theoretical investigations on this subject support the hypothesis of an NO<sup>-</sup> to be involved<sup>19</sup>. Therefore, the reference determinant for our CI-calculations has to be constructed to ensure a proper description of these states. This is achieved by calculating the SCF (high multiplicity) ground state of the system NiO<sub>5</sub><sup>8-</sup>-NO<sup>-</sup> at a quasi infinite distance of  $r(\text{Ni-N}) = 5000 a_0$ . This distance results in a complete separation of cluster orbitals and NO<sup>-</sup> orbitals, so that molecular orbital basis of the NO is especially suited for the description of NO<sup>-</sup>. This fixed set of frozen orbitals is used for the construction of the reference determinant of all CI calculations at shorter distances.

In a previous paper<sup>8</sup> we reported the results of CI calculations in which the CI-space has been generated by performing single and double excitations (CISD) out of the reference determinant within the subspace of the 15 O2p-, the five Ni3d- and the two NO 2 $\pi$ -orbitals of the cluster-adsorbate system. As discussed in detail this procedure results in a proper description of the NO<sup>-</sup>-like charge transfer states, where an electron is transferred out of the cluster to the NO molecule. These states are obtained as highly excited states of the system located at (semiempirically corrected) excitation energies of about 4 eV above the ground state. At excitation energies between 0 eV and 4 eV many states have been found, which can attributed to localized dd-excitations within the Ni<sup>2+</sup>-ions. These states have also been experimentally observed and theoretically assigned<sup>20</sup>. Regardless the fact, that these states are not relevant for the understanding of laser induced desorption, they have to be calculated as lower roots of the CI-matrix, resulting in serious convergence problem when higher roots, corresponding to the charge transfer states, are calculated.

In the present paper we introduce a truncated CI-expansion in which the charge transfer states *and* the ground state are obtained with a similar accuracy compared to the CISD. This expansion omits the dd-excitations, so that only configurations important for the description of the ground state and the charge-transfer states are taken into account. In this expansion the NO<sup>-</sup>-like states turn out to be low excited states, which can be calculated without convergence problems. The reference determinant is divided into four subspaces and the CI-space is generated by constructing all determinants which correspond to the occupation scheme in table 1.

subspace 1 O2p	subspace 2 Ni3d ( $t_{2g}$ )	subspace 3 Ni3d ( $e_g$ )	subspace 4 NO2 $\pi$
30	6	3	0
30	5	4	0
29	6	4	0
30	6	2	1
29	6	3	1
28	6	4	1
30	6	1	2
30	5	2	2
30	4	3	2
30	3	4	2
29	6	2	2
29	5	3	2
29	4	4	2
28	6	3	2
28	5	4	2
27	6	4	2

Table 1. Occupation scheme for the truncated CI-expansion. All determinants matching this occupation scheme are included in the CI-expansion. The numbers in the table correspond to the numbers of electrons within the defined orbital subspaces.

The results of the truncated CI-expansion should be compared with energies of the CISD. Table 2 contains for a tilted geometry ( $r(\text{Ni-N}) = 5.0 a_0$ ,  $\alpha = 45^\circ$ ) the total energies of the  $^2A'$  ground state, the lowest  $^4A'$  excited state and the  $^6A'$  charge transfer state, which is selected as a representative  $\text{NO}^-$ -like state.

CISD		truncated CI	
state	energy / Hartree	state	energy / Hartree
$^2A'$	-2017.503655	$^2A'$	-2017.503600
$^4A'$	-2017.501955	$^4A'$	-2017.501950
$^6A'$	-2017.249822	$^6A'$	-2017.249858

Table 2. Comparison of total energies of CISD and truncated CISD (1 Hartree = 27.21 eV).

It is clearly seen that the computational favourable truncated CI-expansion is sufficiently accurate, because the maximal error turns out to be only 50  $\mu\text{Hartree}$  (1.4 meV). All calculations for excited state potential surfaces described in section 3 have been performed within the truncated CI-scheme.

## 2.2 WAVE PACKET DYNAMICS

The nuclear motion is simulated under the influence of the two PES's of the ground state and of a representative excited state. The dynamics of the nuclei is treated quantum mechanically taking three degrees of freedom into account (distance  $R$  of the centre of mass of the molecule, polar angle  $\alpha$  (tilting angle molecular axis against surface normal), and azimuth angle  $\beta$ ). The time evolution operator is expanded in a series of Chebychev polynomials as proposed by Kosloff<sup>21,22</sup> and the wave function is represented on a three dimensional grid. The grid parameters and further details of the wave packet calculations can be found elsewhere<sup>23</sup>.

Generally, the rotational vibrational ground state wave function of the electronic ground state PES is transferred vertically on the excited state PES and is used as the initial wave function  $\psi_0$  for the wave packet dynamics on the excited state PES starting at the Franck Condon point FC. The desorption scenario is described within a wave packet jumping scheme in which the initial wave packet is transferred after a residence lifetime  $\tau_R$  on the excited state to the ground state. The wave packet is then propagated under the influence of the ground state PES where the desorbing part of the wave packet is analysed after a sufficiently long propagation time  $t_g$ . Velocity distributions are obtained from the desorbing part of the wave packet as momentum space probability distributions in the asymptotic region of the ground state PES. The propagation in potential free space is performed efficiently by a phase shift of the wave packet in momentum space as proposed by Heather and Metiu<sup>24</sup>.

A stochastic incoherent average scheme over  $N$  quantum trajectories distinguished by different residence lifetimes  $\tau_R$  has been applied. This scheme, originally proposed by Gadzuk et al.<sup>25</sup>, has been shown to be a rapidly convergent solution of the Liouville-von Neumann equation for the special case of a constant relaxation probability of the wave packet from the excited PES to the electronic ground state<sup>26</sup>. The constant relaxation probability results in an exponential decay of the negative ion resonance in which the resonance lifetime  $\tau$  enters as a parameter. This single parameter in the average scheme can directly be interpreted as the spectroscopic lifetime of  $\text{NO}^-$ . Any observable  $\langle \hat{A} \rangle_{(t,\tau)}$  for a certain propagation time  $t$  and resonance lifetime  $\tau$  can be obtained as the sum of expectation values  $\langle \hat{A} \rangle_{(t,\tau_R)}$  over  $N$  quantum trajectories weighted by the exponential decay factor (equation 1). In the present paper we used this method in order to calculate incoherently averaged desorption probabilities or state resolved velocity distributions.

$$\langle \hat{A} \rangle_{(t,\tau)} = \frac{\sum_{n=1}^N \exp\left(-\frac{\tau_{Rn}}{\tau}\right) \cdot \langle \hat{A} \rangle_{(t,\tau_{Rn})}}{\sum_{n=1}^N \exp\left(-\frac{\tau_{Rn}}{\tau}\right)} \quad (1)$$

### 3. RESULTS

#### 3.1 POTENTIAL ENERGY SURFACES

By performing truncated CI-calculations described in the last section we were able to obtain many  $\text{NO}^-$ -like charge transfer states of the  $\text{NO-NiO}_3^{8-}$ -system. These states form a quasi-continuum<sup>8</sup>, so that a representative state has to be selected for which a PES is constructed. Analysing the behaviour of the potential energy of the charge transfer states as a function of the relevant degrees of freedom ( $R$ ,  $\alpha$  and  $\beta$ ) it turns out, that most states exhibit a similar behaviour.

As a function of the molecule-surface distance  $R$  the PES for different states are calculated to be very similar and dominated by the Coulomb attraction of  $\text{NO}^-$  and the hole created in the cluster upon charge transfer. This results in a deep potential well with a binding energy of several eV, a long range Coulomb attraction and an equilibrium geometry at smaller distances  $R$  compared to the electronic ground state<sup>8</sup>.

The variation of the potential energy as a function of the azimuth angle is generally very small (10 meV) for all molecule surface distances relevant for desorption dynamics as will be published elsewhere<sup>23</sup>. Therefore this coordinate is not considered in the construction of the PES.

In contrast to this, the variation of the potential energy as a function of the polar angle  $\alpha$  is explicitly taken into account, because it is strongly coupled to the translational motion<sup>9</sup>. Figures 3a and 3b illustrate the behaviour of the potential energy of the six lowest charge transfer states as a function of the polar angle for two selected Ni-N-distances  $r$ .

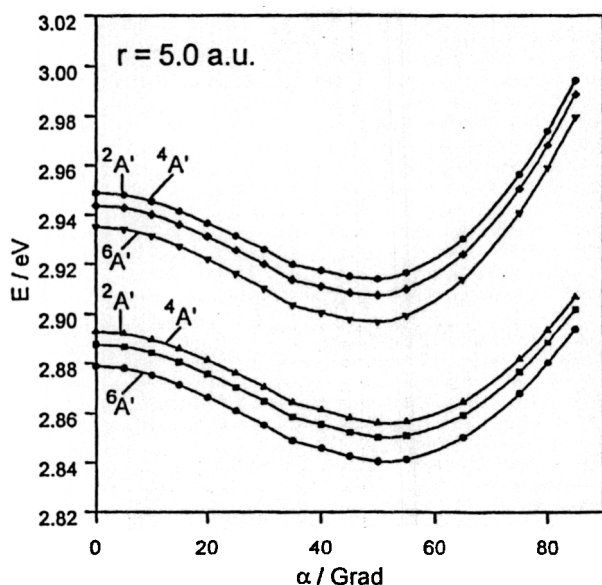


Figure 3a. Potential energy as a function of polar angle  $\alpha$  at a distance of  $r(\text{Ni-N}) = 5.0 a_0$ .

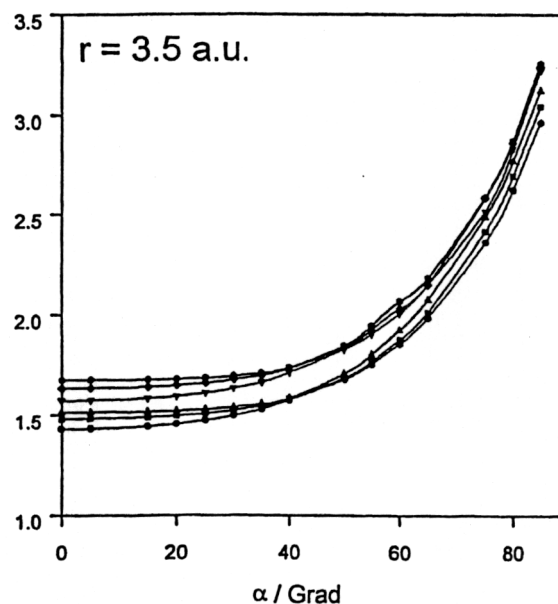


Figure 3b. Potential energy as a function of polar angle  $\alpha$  at a distance of  $r(\text{Ni-N}) = 3.5 a_0$ .

At a Ni-N distance corresponding to the equilibrium distance of the electronic ground state (figure 3a,  $r = 5.0 a_0$ ) the behaviour of the potential energy of the charge transfer states is similar to that of the ground state resulting in a shallow minimum at  $\alpha = 45^\circ$  as has been reported previously<sup>8,9</sup>. The similarity is observed for most of the charge transfer states of which only the lowest states are shown. At short molecule surface distances (figure 3b,  $r = 3.5 a_0$ ) an upright geometry is preferred for all states considered here. For one of these states the behaviour of the potential curves has been analysed<sup>9</sup> as being due to a strong Pauli-repulsion of the spatially extended, diffuse  $\text{NO}^-$ -molecule with the  $\text{O}^{2-}$ -anions within the cluster. Because of the similarity of most calculated potential curves taking one of these states as a representative example can be regarded as a perfectly valid approach. A detailed discussion about exceptions from this typical behaviour will be a topic of a future publication<sup>23</sup>. For technical reasons the selection of the lowest  $6A'$ -state is the most convenient choice.



For this state a two dimensional PES has been constructed by variation of the molecule surface distance  $R$  and the polar angle  $\alpha$ . The pointwise calculated energies have been fitted to an analytical expression, which is given in equation (2)<sup>27</sup> and which is illustrated in figure 4.

$$V(R, \alpha) = -\frac{1}{R} + \sum_{i=0}^{10} \left( \cos^i(\alpha) \cdot \left( \sum_{j=1}^3 a_{ij} \cdot \exp(-b_j \cdot (R - R_0)) + \sum_{k=4}^6 a_{ik} \cdot \exp(-b_k \cdot (R - R_0)^2) \right) \right) \quad (2)$$

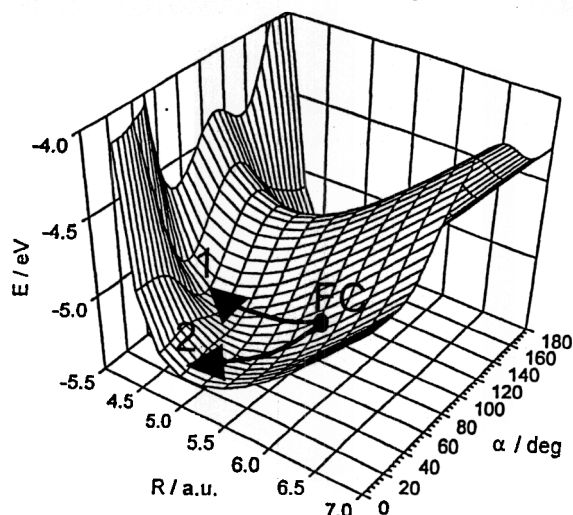


Figure 4. Charge transfer potential energy surface (lowest  ${}^6A'$ -state) as a function of the (center of mass) molecule-surface distance  $R$  and the polar angle  $\alpha$ . FC denotes the Franck-Condon point.

As mentioned before, the gradient of the potential energy results in an acceleration of the molecule towards the surface and a preference of an upright adsorption geometry. At large distances ( $R \geq 10.0 a_0$ ) the PES is dominated just by the Coulomb attraction of the  $\text{NO}^-$  and the ionized cluster resulting in a  $-1/R$  dependence of the potential and an isotropic behaviour in  $\alpha$ . At very short distances ( $R \leq 3.0 a_0$ , not relevant for desorption dynamics) a flat adsorption geometry ( $\alpha = 90^\circ$ ) is preferred because any distortion out of this flat geometry would result in strong Pauli-repulsion. The part of the PES at moderate distances, shown in figure 4, especially reveals the complicated topology being due to a successive transition of the discussed upright geometry preference to the flat geometry at very short distances. The interesting topology of the PES is crucial in understanding the experimental results and could only be obtained by our *ab initio* calculations.

The ground state PES is constructed by adjusting the topology of a potential of Baumeister et al.<sup>28</sup> to *ab initio* results<sup>23</sup>. The potential is illustrated in figure 5 and is characterised by an equilibrium geometry of  $\alpha = 45^\circ$  and  $R = 5.5 a_0$ , where the binding energy of NO on NiO(100) has been scaled to fit the experimentally obtained binding energy of  $0.52 \text{ eV}$ <sup>29</sup>.

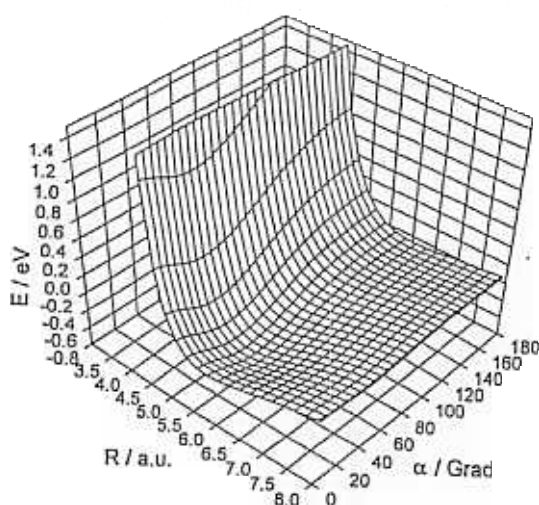


Figure 5. Ground state potential energy surface as a function of the (center of mass) molecule-surface distance  $R$  and the polar angle  $\alpha$ .

### 3.2 WAVE PACKET CALCULATIONS

The two potential energy surfaces introduced in the last paragraph serve as the basis of three dimensional wave packet calculations described in the remainder of the paper. As mentioned in section 2.2 the only parameter in the stochastic wave packet average scheme turns out to be the resonance lifetime  $\tau$ . This parameter has been adjusted once to yield a desorption probability which is comparable with the experimental data (usually a few percent for oxide systems<sup>11</sup>). The desorption probability  $P_{DES}$  is calculated by equation (1) taking the square of the norm of the wave packet in the asymptotic region as the observable to be averaged. It is shown as a function of the resonance lifetime  $\tau$  in figure 6.

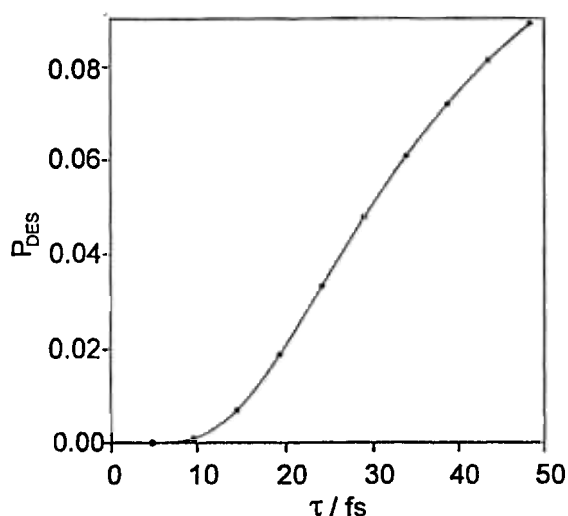


Figure 6. Desorption probability  $P_{DES}$  as a function of the resonance lifetime  $\tau$ .

Figure 7 shows that reasonable desorption probabilities between 1% and 5% are calculated if one assumes a resonance lifetime of  $15 \text{ fs} \leq \tau \leq 35 \text{ fs}$ . Therefore a representative resonance lifetime of 24.19 fs (1000 a.u.) resulting in  $P_{DES} = 3.3\%$  has been chosen in order to calculate the state resolved velocity distributions as the observable of interest. The results are presented in figure 6.

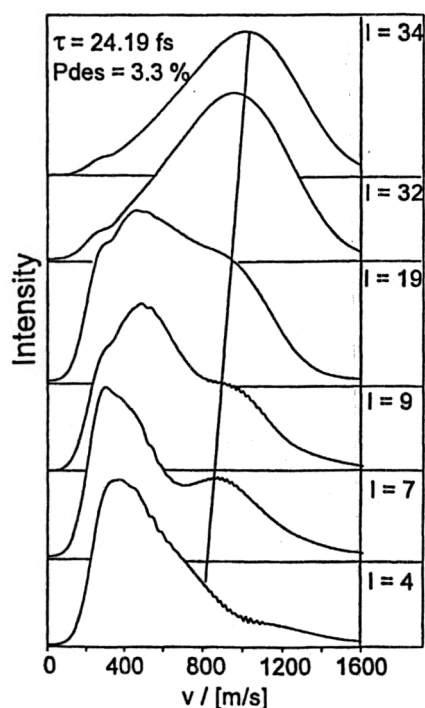


Figure 7. Velocity distributions for a resonance lifetime of 24.19 fs for different rotational quantum numbers  $l$ .



It is clearly seen that all main features of the experimental velocity distributions of figure 1 are reproduced. The distributions are bimodal and turn out to be in the correct velocity range. Additionally, the coupling of rotation and translation in the fast desorption channel is also observed. A simple mechanistic picture to interpret the results is quite difficult to construct, because the results of figure 6 are obtained by averaging momentum space distributions of 80 different quantum trajectories (80 wave packets are necessary to get the sum in equation (1) converged), which have been propagated for different residence lifetimes on two potential surfaces.

Anyway, a simple picture can be constructed which is able to account for the physical mechanism resulting in bimodal velocity distributions. In figure 4 two hypothetical pathways have been indicated, each belonging to a partial wave packet or a swarm of classical trajectories. Pathway 1 belongs to trajectories which take their way along the valley of the excited state PES resulting in a great accumulation of kinetic energy and a relatively small relaxation distance  $R$  after the residence lifetime  $\tau_R$ . On the other hand, other partial wave packets might take pathway 2, which results in an early de-acceleration and a distance of vertical relaxation after the residence lifetime, which is not as close to the surface compared to the trajectories of pathway 1. Because of the difference in the amount of kinetic energy gained in the excited state PES along the two relaxation distances more repulsion is experienced by the wave packet in the ground state potential). A detailed study of phenomena being a possible origin of bimodal velocity distributions has been performed<sup>23</sup>. In this paper only one example is presented supporting the proposed mechanism. Figure 8 shows a velocity distribution of a single wave packet after a residence lifetime of  $\tau_R=52$  fs in the excited state. The distribution is clearly bimodal and an analysis reveals the two maxima being due to the two different pathways indicated in figure 4.

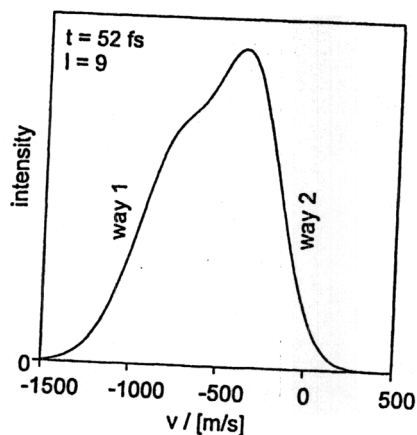


Figure 8. Velocity distribution for a residence lifetime of 52 fs in the excited state for a angular momentum quantum number of  $l = 9$ .

Apart from this appealing picture it has to be pointed out that a quantitative interpretation of the results presented in figure 6 is much more complicated because of the average scheme and the influence of the ground state potential on the nuclear motion after the relaxation. A detailed analysis shows<sup>23</sup> that the influence of the ground state potential is important in understanding details such as the coupling of rotation and translation in the fast desorption channel. Anyway the main result presented in this paper is not affected. The bimodality is due to a bifurcation like deformation of the wave packet as a result of the rotation translation coupling of the potential surfaces. Angular independent model potential yield only monomodal velocity distributions<sup>23</sup>.

#### 4. CONCLUSIONS

In this paper we presented three dimensional wave packet calculations on *ab initio* potential energy surfaces in order to interpret details of experimental results for laser induced desorption of NO on NiO(100). The experiments are quantitatively reproduced and a new mechanistic insight into the physics of the desorption process has been gained.

#### 5. ACKNOWLEDGEMENTS

Financial support from the German-Israeli Foundation (GIF) and the Deutsche Forschungsgemeinschaft (DFG) is gratefully acknowledged. We would like to thank R. Kosloff for many helpful discussion and continuous support.

## 6. REFERENCES

1. F. M. Zimmermann, W. Ho, "State resolved studies of photochemical dynamic at surfaces", *Surf. Sci. Rep.* **22**, 127-247 (1995).
2. D. Menzel, R. Gomer, "Desorption from Metal Surfaces by Low-Energy Electrons", *J. Chem. Phys.* **41**, 3311-3328 (1964).
3. W. Brenig, "Quantum Theory of Electron Stimulated Desorption", *Z. Physik B* **23**, 361-368 (1976).
4. Z. W. Gortel, "Beyond MGR: Wave packet squeezing", *Nuclear Instruments and Methods in Physics Research B* **101**, 11-22 (1995).
5. P. Saalfrank, "Photodesorption of neutrals from metal surfaces: a wave packet study", *Chem. Phys.* **193**, 119-139 (1995).
6. H. Guo, "Two-dimensional wave packet studies of photon-stimulated desorption of NO from a metal surface induced by single and multiple electronic excitations", *J. Chem. Phys.* **106**, 1967-1977 (1997).
7. S.M. Harris, S. Holloway, G. R. Darling, "Hot electron mediated photodesorption: A time-dependent approach applied to NO/Pt(111)", *J. Chem. Phys.* **102**, 8235-8248 (1995).
8. T. Klüner, H.-J. Freund, J. Freitag, V. Staemmler, "Laser-Induced Desorption of NO from NiO(100): *Ab initio* calculations of potential surfaces for intermediate excited states", *J. Chem. Phys.* **104**, 10030-10040 (1996).
9. T. Klüner, H.-J. Freund, J. Freitag, V. Staemmler, "Laser Induced Desorption of NO from NiO(100): Characterization of potential energy surfaces of excited states", *J. Mol. Catal. A*, **119**, 155-163 (1997).
10. T. Klüner, H.-J. Freund, V. Staemmler, R. Kosloff, "Theoretical investigation of laser induced desorption of small molecules from oxide surfaces: A first principles study", *Phys. Rev. Lett.*, submitted
11. T. Mull, B. Baumeister, M. Menges, H.-J. Freund, D. Weide, C. Fischer, P. Andresen, "Bimodal velocity distributions after ultraviolet-laser-induced desorption of NO from oxide surfaces. Experiments and results of model calculations", *J. Chem. Phys.* **96**, 7108-7116 (1992).
12. M. A. van Hove, S.-W. Wang, D. F. Ogletree, G. A. Somorjai, "The state of surface structural chemistry: theory, experiment and results", *Adv. Quantum Chem.* **20**, 1-184 (1989).
13. V. Staemmler, "Open Shell Restricted SCF Calculations for Rotation Barriers about C-C Double Bonds", *Theor. Chim. Acta* **45**, 89-94 (1997).
14. U. Meier, V. Staemmler, "An efficient first-order CASSCF method based on the renormalized Fock-operator technique", *Theor. Chim. Acta* **76**, 95-111 (1989).
15. J. Wasilewski, "Graphical Techniques in the Configuration Interaction Approach Based on Pure Slater Determinants", *Int. J. Quant. Chem.*, **36**, 503-524 (1989).
16. B. Roos, A. Veillard, G. Vinot, "Gaussian basis sets for molecular wavefunctions containing third-row atoms", *Theor. Chim. Acta* **20**, 1-11 (1971).
17. S. Huzinaga, "Approximate atomic functions", preprint, University of Alberta, Canada, 1971.
18. F. M. Zimmermann, "Vibrational Excitation Dynamics in Photodesorption", *Proceedings of the DIET7 conference*, in press.
19. T. Klüner, V. Staemmler, H.-J. Freund, paper in preparation.
20. A. Freitag, V. Staemmler, D. Cappus, C. A. Ventrice Jr., K. Al-Shamery, H. Kühlenbeck, H.-J. Freund, "Electronic surface states of NiO(100)", *Chem. Phys. Lett.* **210**, 10-14 (1993).
21. R. Kosloff, "Time-Dependent Quantum-Mechanical Methods for Molecular Dynamics", *J. Phys. Chem.* **92**, 2087-2100 (1988).
22. H. Tal-Ezer, R. Kosloff, "An accurate and efficient scheme for propagating the time dependent Schrödinger equation", *J. Chem. Phys.* **81**, 3967-3971 (1984).
23. T. Klüner, V. Staemmler, H.-J. Freund, R. Kosloff, paper in preparation.
24. R. Heather, H. Metiu, "An efficient procedure for calculating the evolution of the wave function by fast Fourier transform methods for systems with spatially extended wave function and localized potential", *J. Chem. Phys.* **86**, 5009-5017 (1987).
25. J. W. Gadzuk, L. J. Richter, S. A. Buntin, D. S. King, R. R. Cavanagh, "Laser-excited hot-electron induced desorption: a theoretical model applied to NO/Pt(111)", *Surf. Sci.* **235**, 317-333 (1990).
26. P. Saalfrank, "Open-system quantum dynamics for laser-induced DIET and DIMET", *Surf. Sci.* **390**, 1-10 (1997).
27. The parameters will be distributed to interested readers on request.